iScience

Article

Glacial rock flour enhances phytoplankton growth in phosphorous- and trace metal-depleted environments

Graphical abstract

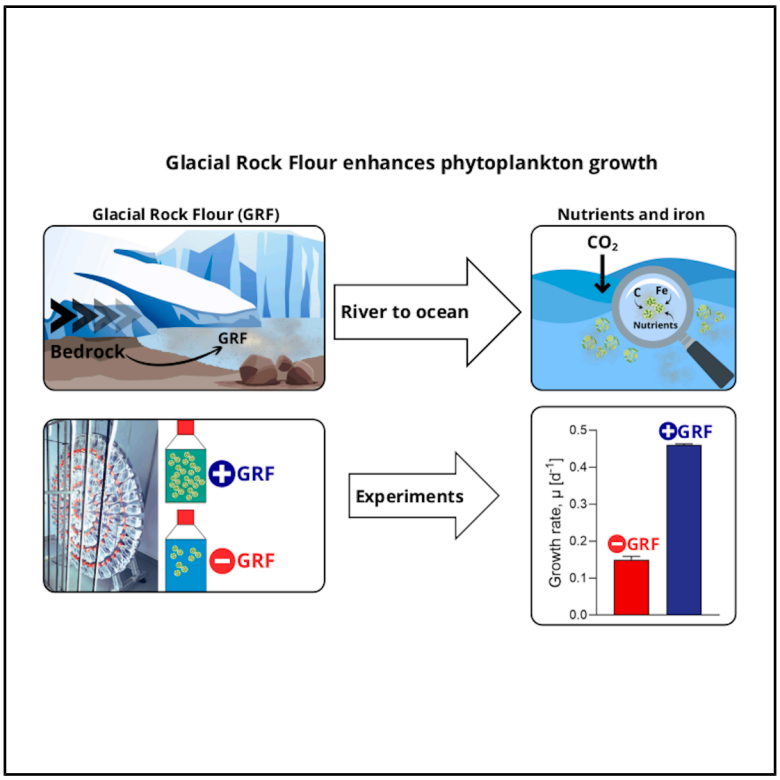

Highlights

- Glacial rock flour contains a significant amount of bioavailable Fe, Mn, and P
- Biological mobilization from glacial rock flour occurs on time scales of days
- Fe from glacial rock flour supports an exponential growth of phytoplankton biomass
- Glacial rock flour is a large source of bioavailable Fe, Mn, and P to the coastal ocean

Authors

Jørgen Bendtsen,
Kristina Vallentin Larsen, Niels Daugbjerg

Correspondence

jorgen.bendtsen@sund.ku.dk

In brief

Marine processes; Biogeochemistry; Marine geochemistry; Aquatic science

Bendtsen et al., 2026, iScience *29*, 115813
May 15, 2026
https://doi.org/10.1016/j.isci.2026.115813

CellPress

iScience

CellPress
OPEN ACCESS

Article

Glacial rock flour enhances phytoplankton growth in phosphorous- and trace metal-depleted environments

Jørgen Bendtsen,[1,2,4,*] Kristina Vallentin Larsen,[1] and Niels Daugbjerg[3]
[1]Centre for Glacial Rock Flour Research, Globe Institute, University of Copenhagen, Øster Voldgade 5-7, 1350 Copenhagen K, Denmark
[2]ClimateLab, Symbion Science Park, Fruebjergvej 3, 2100 Copenhagen Ø, Denmark
[3]Department of Biology, University of Copenhagen, Universitetsparken 4, 2100 Copenhagen Ø, Denmark
[4]Lead contact
*Correspondence: jorgen.bendtsen@sund.ku.dk
https://doi.org/10.1016/j.isci.2026.115813

SUMMARY

Glacial rock flour (GRF) is a fine-grained clay to silt-sized material formed beneath glaciers where bedrock is abraded to fine powder. GRF in meltwater rivers constitutes a major source of continental material to the ocean. Here, we investigate the bioavailability of minerals in GRF and show that GRF increases the biological productivity in incubation experiments with an Arctic green alga, *Pyramimonas diskoicola*. Essential trace metals such as iron and manganese and the macronutrient phosphorus were biologically available from GRF within 3–6 days. In particular, mobilization of iron supplied the exponential growth of microalgal cells as efficiently as from an iron-replete growth medium, whereas growth rates in iron-depleted treatments without GRF were reduced by more than 60%. Hence, GRF stimulates phytoplankton growth and, therefore, constitutes an important nutrient and trace metal source in polar and subpolar coastal areas.

INTRODUCTION

Glacial rock flour (GRF) in Greenland is produced below the ice sheets when an up to several kilometers thick glacier slides and abrades the bedrock.[1,2] The fine-grained rock flour is transported to subglacial hydrological systems, and, eventually, it enters the ocean either via meltwater rivers or directly as subglacial discharge from marine terminating glaciers. Plumes with GRF can be seen from satellites at large distances (>10 km) from river outlets, implying a residence time of several days or weeks in the surface water.[3] Transport of GRF from the Greenland ice sheet makes a substantial contribution of ~8% of the global transport of material from continents to the ocean.[4,5] Simultaneously with increasing meltwater runoff,[6] the transport of suspended material around Greenland is estimated to have increased by more than 56% compared with the 1960–1991 period.[4] This transport is expected to increase further due to global warming,[7] and this may impact biogeochemical cycles and the marine environment in coastal water masses.

GRF consists of a suite of different elements including various nutrients. Applications of GRF on land have shown its potential to stimulate plant growth and increase crop yield,[8,9] and suspended rock flour may similarly impact phytoplankton growth in the ocean. The mineral content of GRF depends on the bedrock composition[2,10] and varies between watersheds below the Greenland ice sheet. Hence, the specific reactivity and potential impact on the marine biota including potential toxic effects,[2,11,12] therefore, depend on the geographical location.

GRF transported to meltwater rivers or entering the ocean as subglacial discharge contains essential nutrients and trace metals for phytoplankton growth, including phosphorus (P),[13] iron (Fe),[14] manganese (Mn), and other trace metals.[15] Incubations of GRF from Greenland and Svalbard have shown that Fe, Mn, and silica can be released during a 3-week period.[16] Biological incubation experiments have shown that GRF rich in Fe(II) from glaciated areas in South America stimulates the growth of phytoplankton.[17] Incubation experiments with GRF from Greenland and natural phytoplankton communities from the subtropical Atlantic have also showed an increase in the photosynthetic efficiency and chlorophyll *a* concentrations.[18] Collectively, these studies have shown that GRF can be a source of trace metals and also stimulate phytoplankton growth. Transport by ocean currents[19,20] or atmospheric dust,[21] therefore, provides potential supplies of nutrients and trace metals to the open ocean.

However, it is currently unknown to what extent the specific GRF components stimulate phytoplankton, and this is the primary focus of this study. Here, we analyzed the impact of GRF on growth of an arctic green alga, with a special focus on its capacity for supplying Fe, Mn, and P for phytoplankton growth. We designed a set of incubation experiments to identify the relative reactivity of these elements. GRF was collected from a sediment at a shallow marine deposit close to a major meltwater river outlet in Nuuk fjord (Figure 1). Different treatments address the potential influence of the seawater composition, e.g., dissolved nutrients and organic compounds, and the influence of different

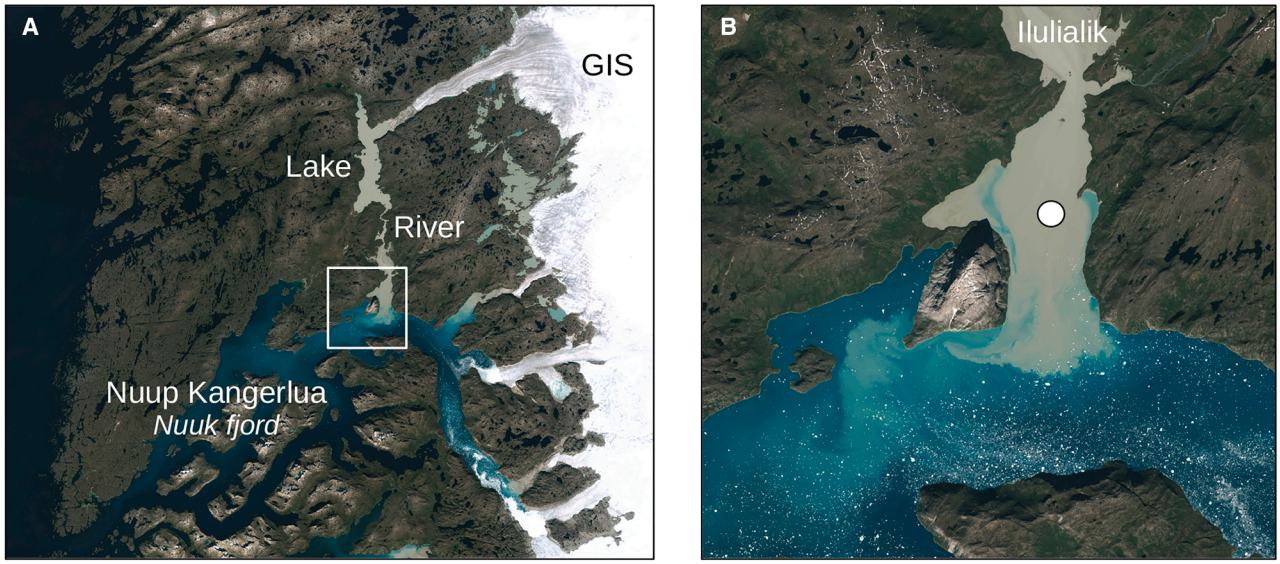

Figure 1. Sampling location

(A) Meltwater is transported from the Greenland Ice Sheet, via Lake Tasersuaq and a meltwater river to the narrow strait at Ilulialik (white square) and into Nuup Kangerlua (Nuuk fjord).

(B) Sampling location of GRF. Source: Spot and Sentinel 2 satellite images from https://dataforsyningen.dk; (A) Jun–Aug 2020; (B) Aug 2022.

sampling methods and postprocessing of the GRF. The relative amount of consumed elements from the GRF was estimated using a mass balance model, and finally, the impact of GRF on ocean productivity and its potential as a means of action in marine carbon dioxide removal (mCDR) applications are discussed.

RESULTS AND DISCUSSION

GRF and cell abundance

Biological mobilization of Fe, Mn, and P and the role of EDTA complexation with Fe were identified from a time series of cell abundance in the various treatments in experiments I–IV (Table 1). The treatments contained different compositions of an optimal growth media with nitrogen (N), P, vitamins (V) and trace metals (T); treatments with all components are referred to as NPVT. Treatments without specific compounds, for example, Fe, are referred to as NPVT-Fe, i.e., a growth media with all trace metals except Fe (see STAR Methods).

Fe limitation and cell abundance

Treatments without Fe (i.e., the NPV and NPVT-Fe treatments in experiments I–III, shown with pale brown and red, respectively, in Figures 2A–2C; Table 1) were strongly influenced by Fe limitation. The NPV and NPVT-Fe treatments showed very little growth during the incubations compared with incubations with all trace metals (NPVT, shown with gray) or GRF (i.e., NPV + GRF and NPVT-Fe + GRF, shown with light and dark blue, respectively). In treatments without Fe, the growth ceased after 6–9 days. Differences between the Fe-limited NPV and NPVT-Fe were relatively small in all experiments, and the low growth rates with final cell abundances of $\sim 10^3$–10^4 cells mL^{-1} in both treatments showed a large impact of Fe limitation on growth.

Treatments where Fe or GRF was included obtained much higher cell concentrations, with peak values above 10^5 cells mL^{-1}, i.e., 1–2 orders of magnitude larger than those under the Fe-depleted treatments. The final concentrations above $\sim 2 \times 10^5$ cells mL^{-1} after day 15 tended to collapse because of high pH values (>9.5) at the end of the incubations due to the greater uptake of dissolved inorganic carbon. Treatments with GRF were all comparable to treatments with NPVT. Hence, NPV + GRF and NPVT-Fe + GRF treatments showed a similar temporal trend as the NPVT treatment in experiments I–III. This demonstrated that GRF compensated for the omitted Fe in the NPVT-Fe treatments.

Mn limitation and cell abundance

Mn had a significant ($p = 0.02$) influence on cell abundance (Figure 2C). After 15 days, the concentration under NPVT treatment was $\sim 2.4 \pm 0.16 \times 10^5$ cells mL^{-1}, whereas the treatment without Mn only had $1.9 \pm 0.17 \times 10^5$ cells mL^{-1} (NPVT-Mn treatment is shown in dashed light purple in Figure 2C). This corresponded to a 22% reduction in cell concentration due to the lack of Mn. In treatments where Mn was omitted and GRF was added (i.e., NPVT-Mn + GRF is shown in dashed purple), the reduction was only 2% and not significantly different from that under NPVT. This demonstrated that Mn limitation had a significant impact on cell abundances, and mobilization of Mn from GRF could partly compensate for Mn in those treatments where Mn was omitted.

P limitation and cell abundance

Removal of P from the growth media (i.e., NVT, shown with light brown in Figure 2D) also had a significant ($p < 10^{-4}$) impact on cell abundance. Treatments without P resulted in a cell concentration of only 2.2×10^4 cells mL^{-1} after 15 days, whereas the

Table 1. Description of experiments and treatments

Exp. no.	Batch water	Glacial rock flour	Focus element
I	oceanic	2024-material	Fe, EDTA
II	oceanic	2015-material	Fe
III	shelf sea	2015-material	Fe, Mn
IV	shelf sea	2015-material	P

Treatment ID	Description of treatment	Focus and experiment no.
NPVT	Full L1-media include N, P, vitamins (V), and all trace metals (T)	Fe, Mn, and P: I-IV
NPV	as NPVT but without trace metals	Fe: I–III
NPV + GRF	as NPV and where GRF was added, i.e., 0.326 g GRF L^{-1}	Fe: I–III
NPVT-Fe	as NPVT but without Fe	Fe: I–III
NPVT-Fe + GRF	as above and where GRF was added, i.e., 0.326 g GRF L^{-1}	Fe: I–III
NPVT-Mn	as NPVT but without Mn	Mn: III
NPVT-Mn + GRF	as above and where GRF was added, i.e., 0.326 g GRF L^{-1}	Mn: III
NPVT-E	as NPVT but without EDTA	Fe and EDTA: I
NPVT-E-Fe	as NPVT but without EDTA and Fe	Fe and EDTA: I
NPVT-E-Fe + GRF	as above and where GRF was added, i.e., 0.326 g GRF L^{-1}	Fe and EDTA: I
NVT	as NPVT but without P	P: IV
NVT + GRF	as NVT and where GRF was added, i.e., 0.326 g GRF L^{-1}	P: IV

Description of batch water origin in experiments I–IV and the applied Fe, Mn, EDTA, and P in the associated treatments. Batch water is identified by its origin (oceanic: Iceland Basin or Shelf Sea: entrance to the Baltic Sea), the source of GRF is Ilulialik in Nuuk Fjord, Greenland, and time of collection and the focus on various elements in GRF and the growth media in each experiment. Different treatments are associated with each experiment and abbreviated according to the growth media (e.g., NPVT implies nitrogen, phosphorus, vitamins, and trace metals are included; NPTV-Fe implies growth media comprising all trace elements, except Fe; NPVT-Fe + GRF implies the growth media except Fe and addition of GRF. The focus of each treatment and the corresponding experiment(s) are listed.

corresponding concentration in the NPVT treatment was 2.0×10^5 cells mL^{-1}. This showed that growth was strongly limited by P availability. Addition of GRF to the batch solution (i.e., NVT + GRF, shown with brown in Figure 2D) more than doubled the cell concentration after 15 days (i.e., 5.7×10^4 cells mL^{-1}) in comparison with the NVT treatments. Hence, a significant (p = 0.001) amount of P was also mobilized from GRF and able to partly compensate for the lack of P in these treatments. P mobilization from GRF was not able to compensate fully for the absence of phosphate, and the cell abundance was only 29% of the NPVT concentration after 15 days.

EDTA-Fe complexation and cell abundance

Fe complexation with EDTA provides a buffer of bioavailable Fe for cell growth during the incubations. The EDTA treatments were designed to investigate the potential impact of EDTA on Fe mobilization from GRF and, in particular, to exclude the possibility that mobilization rates in the GRF experiments could be associated with EDTA in the growth media (Table 1). A reference treatment with NPVT without EDTA (i.e., NPVT-E shown with dashed light purple in Figure 2A) was, therefore, compared with a treatment without Fe referred to as NPVT-E-Fe (shown with dashed purple) and a similar treatment where GRF was added (i.e., NPVT-E-Fe + GRF, shown with dark purple). Treatments without EDTA at day 18 were not significantly different from the NPV treatment, and removing Fe also did not make any significant change. Contrarily, adding GRF made a significant difference, i.e., NPVT-E-Fe + GRF resulted in 2.0×10^5 cells mL^{-1} at day 18 (i.e., different from the NPVT-E-Fe treatment with 1.8×10^4 cells mL^{-1}, $p < 10^{-3}$). This was similar to the reference NPVT and NPVT-Fe + GRF treatments and demonstrated that the presence of EDTA in the growth media had no significant impact on the mobilization rate of Fe determined from the GRF experiments. Hence, we do not expect a bias of our result due to the presence of EDTA in the media. It should be noted that the functioning of EDTA as an Fe ligand may be compensated for by the natural occurrence of dissolved organic matter in the applied seawater.[22–24]

GRF and growth rates

Growth rates in all experiments were analyzed during days 3–15 (Figure 3). In general, linear regression of treatments with all trace metals or addition of GRF showed a strong correlation (R^2 ~0.97–0.99, n = 5), and this supported that the growth rate (μ, d^{-1}) was well represented by a constant value during the growth phase of the experiments (Table 2).

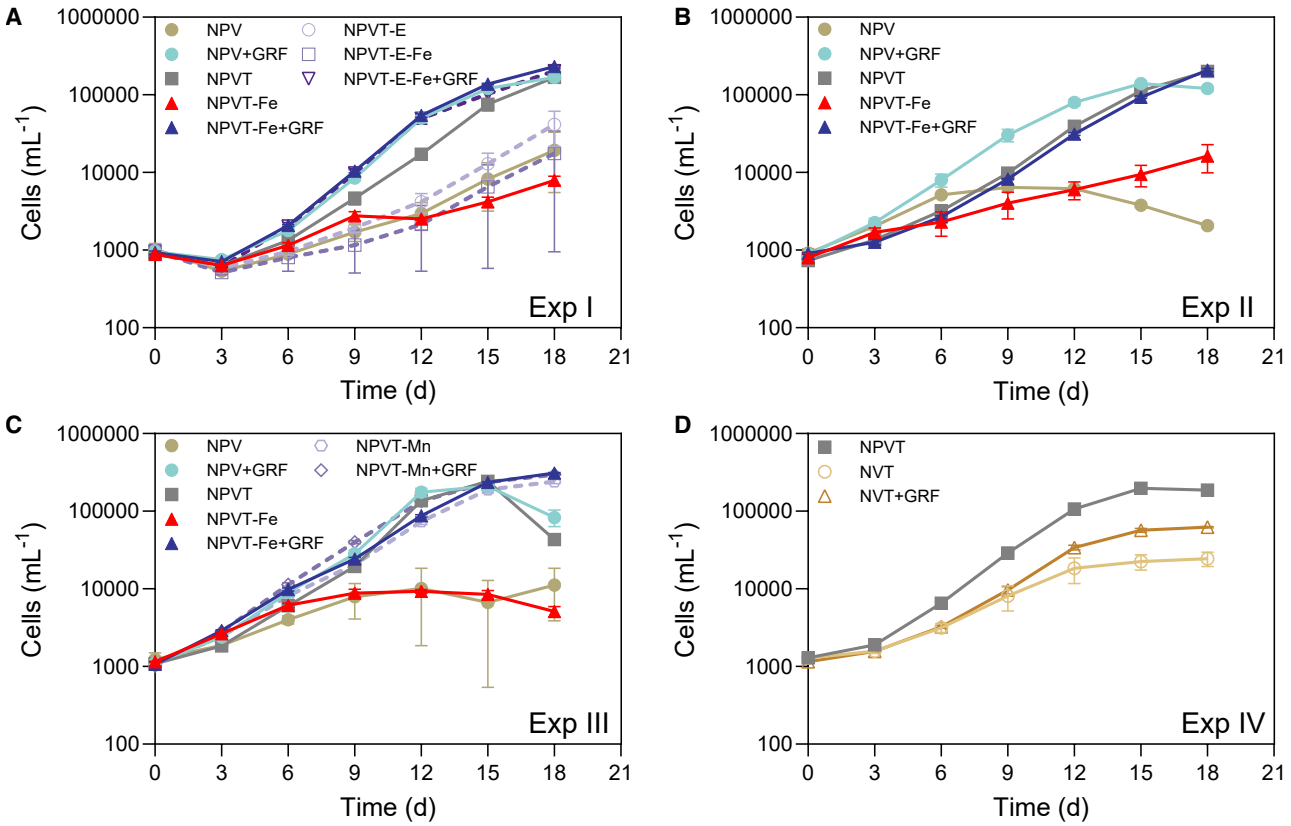

Figure 2. Time series of cell concentrations

Time series (mean ± SEM) of cell concentrations between day 0 and day 18 in the four experiments (mean ± SEM). (A) experiment I, (B) exp. II, (C) exp. III, and (D) exp. IV. Standard errors are shown as error bars (some less than symbol size).

Bioavailable Fe and growth rates

Treatments without Fe or GRF showed significantly lower growth rates, and, in general, caused cessation of growth before day 15 (i.e., NPV and NPVT-Fe shown with red and brown, respectively, in Figures 3A–3C). This showed that Fe was particularly important for the growth rates and could explain the limitation in these treatments. The ANOVA of the five treatments in experiments I–III between day 3 and day 15 (i.e., NPVT, NPV, NPV + GRF, NPVT-Fe, and NPVT-Fe + GRF) showed that there were no significant differences among the three experiments with all trace metals or addition of GRF (i.e., NPVT, NPV + GRF, and NPVT-Fe + GRF in each experiment, shown with gray, light blue, and blue, respectively). Growth rates varied between 0.35 and 0.45 $days^{-1}$ in these experiments. The importance of Fe among the trace metals was further supported by the similarity between NPVT-Fe and NPV treatments under which the growth rates were less than 0.2 $days^{-1}$ (Table 2). Growth rates in the Fe- or GRF-free incubations were significantly different from those under incubations with Fe and GRF. A direct comparison between treatments without Fe and without/with GRF (i.e., NPVT-Fe vs. NPVT-Fe + GRF, shown as red and blue, respectively, in Figures 3A–3C) showed that growth rates in the Fe-depleted treatments decreased by more than 60%, whereas no significant difference was found between NPVT and the treatments with GRF, and the mobilization rate of Fe from GRF could supply plankton uptake comparable with Fe consumption in the NPVT treatments which were Fe replete.

Bioavailable Mn and growth rates

Lack of Mn had a moderate effect on growth rates (Figure 3C); however, cell abundances were significantly different among the treatments. Growth rates varied between 0.36 $days^{-1}$ (NPVT-Mn) and 0.38 $days^{-1}$ (NPVT-Mn + GRF) and were lower than the NPVT growth rates of 0.43 $days^{-1}$ (Table 2). However, the ANOVA of growth rates between day 3 and day 15 of NPVT, NPVT-Mn, and NPVT-Mn + GRF treatments (Table 2) showed no significant differences, although cell numbers were significantly higher when GRF was added.

Bioavailable P and growth rates

Lack of P in the NVT treatments reduced the growth rate significantly (Figure 3D). Addition of GRF to the treatments without P also resulted in an increased growth rate. The ANOVA between NPVT, NVT, and NVT + GRF showed a significant difference between treatments with and without P. A direct comparison between treatments with and without GRF (i.e., NVT + GRF and NVT) showed a growth rate reduction of ~20% in the treatments with GRF, whereas the growth rate in the NVT treatment was reduced by more than 40%. Thus, comparing growth rates of

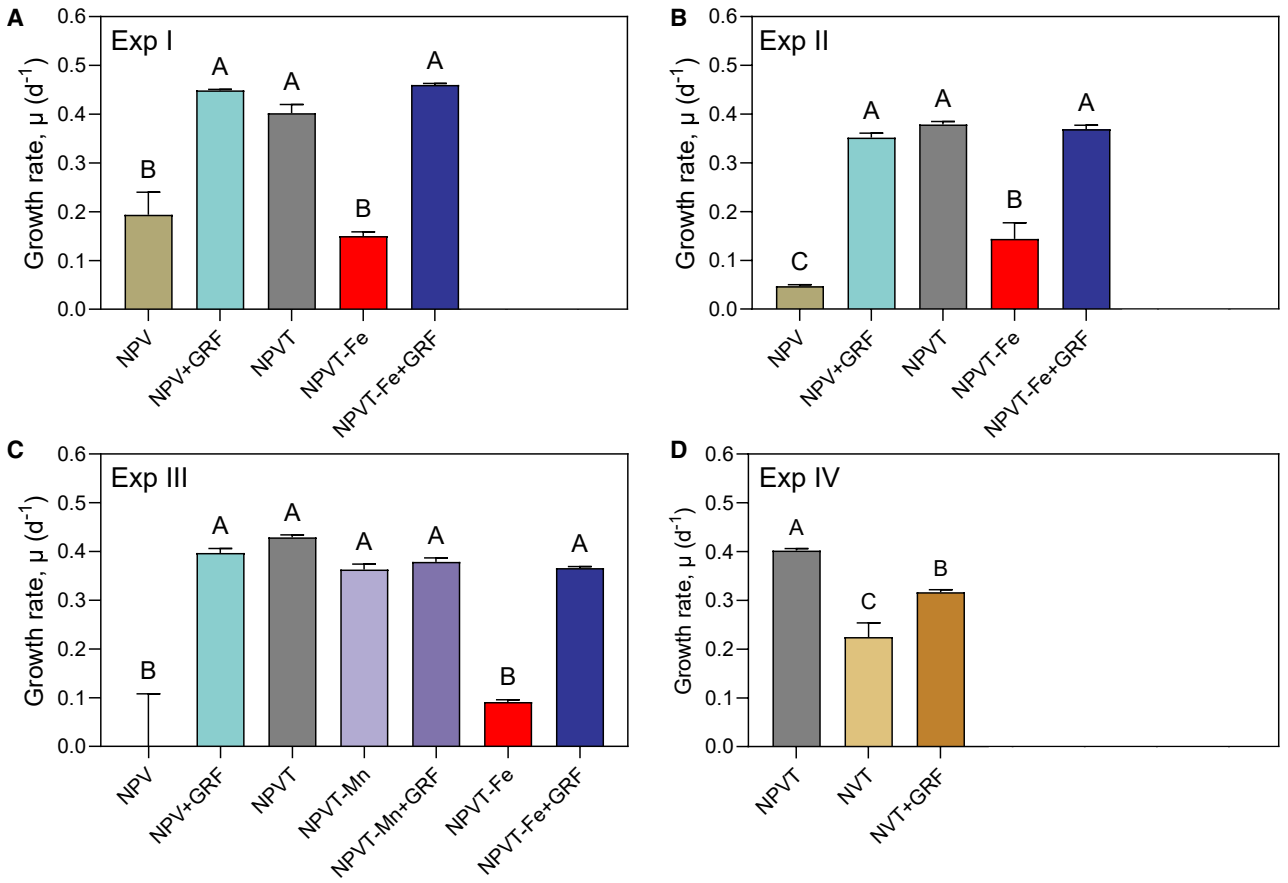

Figure 3. Growth rates in the experiments

Growth rate (μ) during days 3–15 in the four experiments (mean ± SEM). (A) experiment I, (B) exp. II, (C) exp. III, note that the growth rate of NPV is close to zero, and (D) exp. IV.

treatments with and without GRF indicated a significant mobilization of P from GRF (Figure 3D, NVT vs. NVT + GRF).

GRF and photosynthetic efficiency

Photosynthetic efficiency (i.e., Fv/Fm) showed relatively low variation during the experiments, except from initial changes in the first three days (Figure 4). This initial response was related to the onset of the experiment and acclimation of the cells in the lag phase. Treatments without trace metals or GRF (i.e., NPV and NPVT-Fe shown with brown and red, respectively, in Figures 4A–4C) resulted in values that tended to remain below 0.25. Treatments with trace metals or GRF (i.e., NPVT, NPVT-Fe + GRF, and NPV + GRF shown with gray, blue, and light blue, respectively, in Figures 4A–4C) had relatively high values

Table 2. Growth rates in experiments and treatments

Exp. no	NPVT	NPV	NPV + GRF	NPVT-Fe	NPVT-Fe + GRF
I	0.402 ± 0.018 (0.97–0.99)	0.194 ± 0.046 (0.97–0.99)	0.449 ± 0.002 (0.98–0.99)	0.150 ± 0.009 (0.77–0.97)	0.460 ± 0.003 (0.99)
II	0.379 ± 0.006 (0.99)	0.047 ± 0.003 (0.21–0.33)	0.352 ± 0.009 (0.98–0.99)	0.144 ± 0.033 (0.71–0.99)	0.369 ± 0.008 (0.97–0.98)
III	0.429 ± 0.005 (0.98)	0.001 ± 0.107 (0.39–0.82)	0.397 ± 0.009 (0.97–0.98)	0.091 ± 0.005 (0.56–0.99)	0.366 ± 0.003 (0.99)
Exp. no	NPVT	NPV	NPVT-EDTA	NPVT-EDTA-Fe	NPVT-EDTA-Fe + GRF
I:EDTA	as I	as I	0.244 ± 0.029 (0.94–0.99)	0.101 ± 0.093 (0.20–0.99)	0.446 ± 0.014 (0.98–0.99)
Exp. no	NPVT	NPV	NPV + GRF	NPVT-Mn	NPVT-Mn + GRF
III:Mn	as III	as III	as III	0.363 ± 0.011 (0.99)	0.379 ± 0.008 (0.98–0.99)
Exp. no	NPVT	NVT	NVT + GRF	–	–
IV	0.402 ± 0.004 (0.98)	0.225 ± 0.029 (0.90–0.95)	0.317 ± 0.005 (0.98)	–	–

Sensitivity and statistics ($n = 5$, range of R^2 for linear regressions shown in parentheses) of growth rates (μ, day^{-1}, SEM) to iron, manganese, and phosphorus between day 3 and day 15.

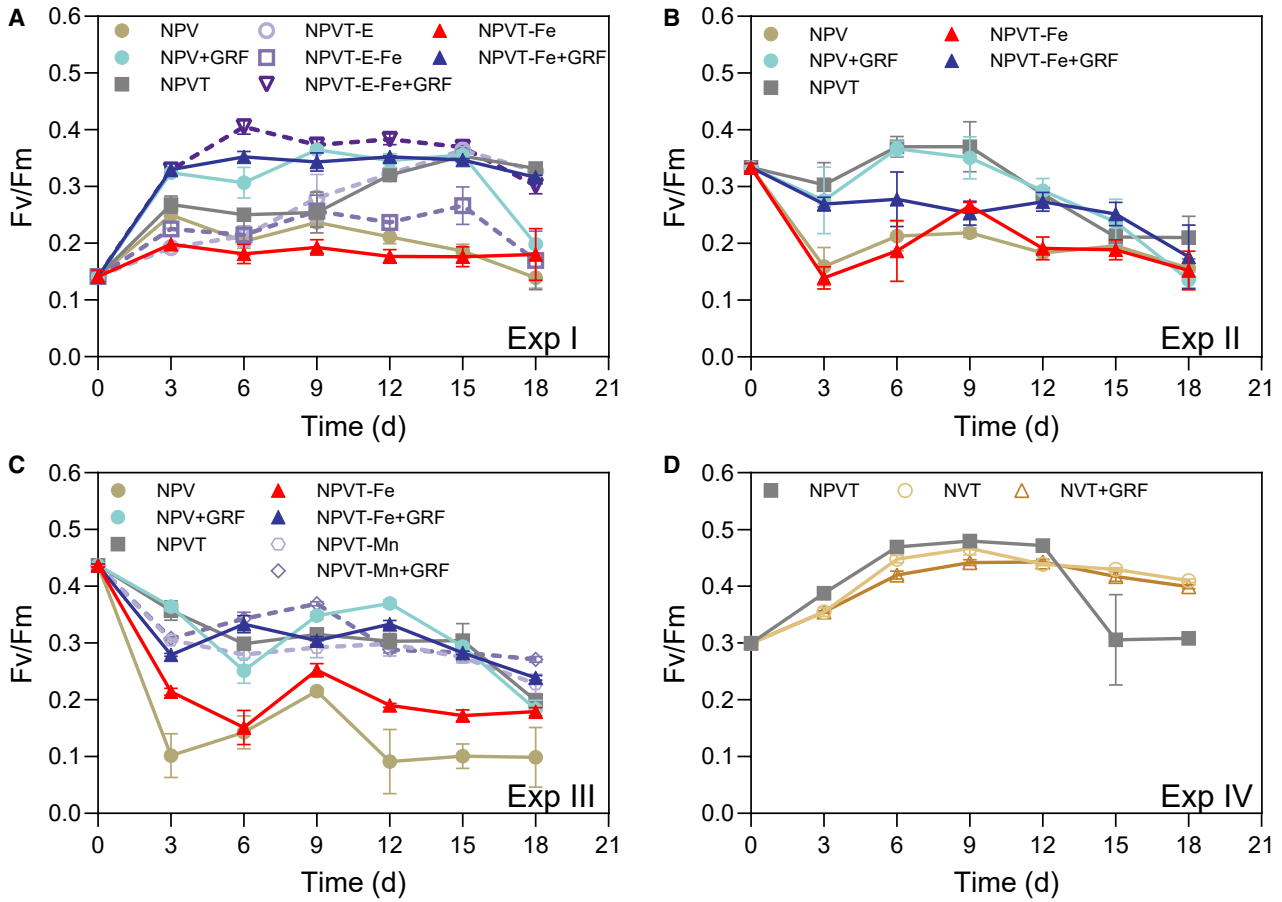

Figure 4. Time series of variable fluorescence

Time series of Fv/Fm between day 0 and day 18 in the four experiments (mean ± SEM). (A) experiment I, (B) exp. II, (C) exp. III, and (D) exp. IV.

between 0.25 and 0.5, which were significantly higher than those under treatments without trace metals or GRF. The high Fv/Fm values tended to decrease after day 15, and this could be explained by the high cell abundances and high pH-values. The low Fv/Fm in the Fe-depleted treatments implied a weak photosynthesis response to light, in accordance with the known importance of Fe for photosynthetic efficiency.[25] The Fv/Fm supported that a significant Fe supply was provided by the GRF.

Mn had a smaller impact on the temporal changes in Fv/Fm, and, in accordance with the similarity in growth rates, there were no significant difference in Fv/Fm between NPVT, NPVT-Mn, and NPVT-Mn + GRF treatments (Figure 4C). However, the Fv/Fm in treatments without Mn but with GRF tended to be higher than in the treatments without Mn. This is in accordance with higher cell abundances in this treatment (i.e., NPVT-Mn + GRF compared with NPVT-Mn).

Treatments without P but with all trace metals and with/without GRF showed a similar response as NPVT, and this showed that the photosynthetic efficiency was not significantly affected in these Fe-enriched treatments (Figure 4D). However, both treatments without P tended to be a little lower than the reference NPVT treatment, except after day 12 where the pH was higher than 9.5. The relatively high pH in the NPVT treatments, compared with pH < 8.5 in the two other treatments, resulted in a decrease in Fv/Fm.

Treatments with GRF but without EDTA and Fe had a relatively high Fv/Fm values that were even significantly higher than those under the reference NPVT treatment between day 3 and day 12 (Figure 4A). Fv/Fm in the treatment without Fe (i.e., NPVT-E-Fe) was relatively low during day 3–12 in accordance with the other Fe-depleted treatments. Fv/Fm in the treatments without EDTA (NPVT-E) was significantly lower than the treatment where GRF was added (NPVT-E + GRF) until day 15. These results support that the impact of EDTA on GRF mobilization was negligible.

Mass balance of biological Fe uptake

The experiments showed a significant impact of Fe depletion on cell abundances, growth rates, and photosynthetic efficiency. This is in accordance with the relatively high cellular Fe quota in phytoplankton.[26,27] However, only a minor impact of Mn and P depletion on photosynthesis was observed, and this indicated that growth was not severely limited by these elements. This could possibly be explained by the presence of larger pools of Mn and P in the batch water in relation to the required compounds for growth. The large physiological impact of Fe on cell growth and photosynthesis in the Fe-depleted experiments

showed that the bioavailable pool of Fe from the background concentration in the batch water was almost completely consumed. Below, we apply this result to constrain a mass balance model of biological Fe uptake.

The biological Fe consumption in relation to the total Fe content in the added GRF (i.e., in a concentration of 0.326 g L^{-1}) can be estimated by a mass budget model of the mobilized Fe. Each cell was assumed to contain a certain amount of Fe (γ_{Fe}, mole Fe $cell^{-1}$) and nutrients (e.g., mole nitrogen per cell, γ_N), and the total uptake could, thereby, be determined from the difference between the initial number of cells (n_{ini}) and the maximum cell number (n_{max}) during the incubation period. The cellular Fe content has been determined for various green algae, and we assume that the Fe content of the species *Pyramimonas parkeae*, which belongs to the same genus as *P. diskoicola* applied in this study, was representative. Molar ratios for this species have been reported[28] as Fe:P:N of $15.4 \cdot 10^{-3}$:1:17.6, e.g., a molar ratio of Fe:P of $15.4 \cdot 10^{-3}$ and a Fe:N ratio of 0.875 mmol mol^{-1}. The nitrogen content of the cell varies with the cell volume, and the volume was estimated by applying the reported[29] dimensions of *P. diskoicola* (w/l = 5.1/8.3 μm), resulting in an average cone-shaped cell volume of 56.5 μm^3. Nitrogen content was estimated from typical N:volume relations.[30] This implies an estimated Fe content per cell of $\gamma_{Fe} = 2.27 \cdot 10^{-16}$ mol Fe $cell^{-1}$.

There were 3 sources of Fe in the experiments: (1) Fe added from the L1 growth media (Fe_{L1}), (2) Fe mobilized from GRF (Fe_{GRF}), and (3) Fe in the initial batch water with natural seawater and the small inoculum with the initial phytoplankton biomass (Fe_{bw}). Note that Fe_{bw} includes Fe from both the applied seawater and from the small inoculum. The total bioavailable Fe in the incubations was then determined as follows: $Fe_{tot} = Fe_{bw} + Fe_{L1} + Fe_{GRF}$.

The NPVT-Fe treatment made a special subset of the treatments where the only source of Fe was the Fe present in batch water and the small inoculum (i.e., Fe_{L1} and Fe_{GRF} were zero). The increase in cell concentration (Δn) in these treatments solely accounted for the bioavailable Fe in the batch water and the small inoculum (i.e., Fe_{bw}). This Fe pool could be estimated from the difference between the maximum and initial cell numbers from the NPVT-Fe treatment (Δn_{bw}), i.e., $Fe_{bw} = \gamma_{Fe}\ \Delta n_{bw}$. The initial cell concentration in experiment I of 883 ± 27 cells mL^{-1} (SEM, standard error of the mean) increased to a maximum value of 7897 ± 1018 cells mL^{-1}, and the estimated Fe uptake based on this difference in cell concentration then corresponded to 1.6 ± 1.5 nM Fe (i.e., originating from the batch water and the small inoculum). The corresponding estimates for Fe content in the batch water of the NPVT-Fe treatments in experiments II and III were 3.5 and 1.8 nM, respectively.

Similarly, the NPVT-Fe + GRF treatments contained Fe only from the batch water, the small inoculum, and the added GRF (i.e., $Fe_{L1} = 0$), and the total Fe uptake from GRF (Fe_{GRF}) could then be estimated from the difference between the maximum and initial cell numbers (Δn_{GRF}) as: $Fe_{GRF} = \gamma_{Fe}\ \Delta n_{GRF} - Fe_{bw}$. Hence, Fe_{GRF} represents the mobilized Fe during the incubation period and is, thereby, a minimum estimate of the total bioavailable Fe from the added GRF.

The estimated Fe_{bw} in the three experiments varied between 1.6 and 3.5 nM, where the Icelandic Basin water had the lowest concentration. The batch water Fe concentrations were comparable with previous observations of surface water from the Iceland Basin[10] and the North Sea[31] ranging between ~0.1 and 2 nM. Fe_{bw} also contained Fe from the small inoculum and possibly from contamination during the handling procedure; however, the consistency among the replicates in the incubations and the relatively low estimated F_{bw} support that these Fe sources can be assumed to have a minor impact on the growth.

Fe_{GRF} ranged between 44 and 68 nM in the three experiments, with an average of 54 nM, which was, thereby, more than an order of magnitude larger than the bioavailable Fe from the batch water. Comparison with the Fe content in GRF[32] (~8.6 wt % of Fe_2O_3 or 0.5 mmol (g GRF)$^{-1}$), corresponding to a concentration of ~0.4 mM Fe, if fully dissolved in the batch water, showed that only a tiny fraction (i.e., 44–68 nM from a total pool of 0.4 mM) of the total Fe content in the added GRF was consumed during the experiments. In summary, the mass budget model shows that a significant amount of Fe was mobilized from the GRF in comparison with similar treatments without GRF.

Impact on coastal cycling of Fe

Glacial meltwater rivers have a relatively high concentration of dissolved Fe.[14,33,34] However, a major part of dissolved and particulate Fe is removed in the transition zone from the river outlet toward more saline coastal water masses[31,35–38] due to increased flocculation at high salinities.[39] The transport of suspended GRF thereby constitutes a pathway of continental nutrients and trace metals to the coastal ocean.[19] Chemical and biological processing of sedimented GRF adds to dissolved fluxes across the sediment-water interface and may enrich bottom water masses with Fe[40] or enhance its bioavailablity.[41] Considering the large transport of suspended material from the Greenland ice sheet and the rapid biological mobilization of Fe from GRF, our results suggest that a pelagic biological-mediated pathway of Fe, Mn, and P supplied by GRF may be an important additional component of nutrient and trace metal cycling in subpolar seas.

GRF and mCDR

The ocean constitutes a large reservoir of dissolved carbon and contains ~40 times the current mass of ~870 Gt of carbon in the atmosphere.[42] Increasing ocean carbon storage by a few percent would make a substantial contribution to bringing atmospheric CO_2 down to levels that are within planetary boundaries (i.e., ~350 ppm) and thereby sustain the stability and resilience of the Earth system.[43] Fe is limiting productivity in large areas of the ocean,[27,44] and the addition of Fe or other nutrients to the surface ocean has, therefore, been considered in relation to mCDR.[45–47]

Our experiments demonstrated that GRF rapidly stimulates phytoplankton growth. GRF is also available in large quantities from sedimentary deposits around Greenland.[1,48] Dispersal of GRF in trace metal- and/or nutrient-depleted ocean areas[27,49,50] could, therefore, increase ocean productivity, consume dissolved inorganic carbon, and thereby increase oceanic CO_2 uptake. The net effect would, in principle, be similar to previous field

studies of Fe fertilization[51–53] or as simulated in model studies of the addition of Fe or macronutrients.[45,54] However, several unknown factors may limit the efficacy of this mCDR approach in relation to the export of carbon and the sequestration time of remineralized organic carbon in the deep ocean.[55–57] Our experiments support that growth of phytoplankton can be stimulated by GRF, and this is the first step for a marine GRF application for CO_2 removal; however, the overall impact on the biological pump needs further investigations.

Impact of GRF on primary production

GRF contains significant amounts of bioavailable Fe, Mn, and P that can rapidly be mobilized for phytoplankton growth on time scales within 3-6 days. Fe was mobilized from GRF at a rate that could supply exponential growth of cells as efficiently as from an Fe-replete growth medium. Significant amounts of Mn and P were also found to be mobilized, although they could only partly compensate for the lack of these elements. This implies that GRF has a large potential for supplying primary producers in the ocean with these essential nutrients and trace metals.

Limitations of the study

Two sources of GRF, collected at the same location in 2015 and 2024, were analyzed in the experiments, and they were assumed to be representative of sedimented GRF in the marine deposit. The general similarity between experiments with GRF (e.g., NPV + GRF in experiments I–III resulted in growth rates ranging between 0.35 and 0.45 $days^{-1}$, Table 2) and the relatively large and significant difference between experiments without GRF (i.e., NPV with growth rates between ~0 and 0.19 $days^{-1}$) supported that the bioavailable trace metal content is about the same in the two GRF sources. The similar response to GRF from the two different sampling periods of GRF, i.e., experiment I versus experiments II–III also supported that contamination during sampling, postprocessing, and experimental setup could be considered to be of minor importance.

The biological response to Fe mobilization from GRF by the green algae *P. diskoicola* may differ from that by other phytoplankton species where the GRF content of other minerals, e.g., silicate, also may impact the growth rate. However, Fe is an essential element for all phytoplankton species, and, therefore, we consider GRF to be a general potential trace metal and P source for phytoplankton growth, although there likely will be a species-dependent sensitivity.

RESOURCE AVAILABILITY

Lead contact

Requests for further information should be directed to and will be fulfilled by the lead contact, Jørgen Bendtsen (jorgen.bendtsen@sund.ku.dk).

Materials availability

This study did not generate new unique materials.

Data and code availability

- Data: All data reported in this publication will be shared by the lead contact upon request.
- Code: This article does not report any original code.
- All other items: Any additional information required to reanalyze the data reported in this paper is available from the lead contact upon request.

ACKNOWLEDGMENTS

This study was supported by the Novo Nordisk Foundation (NNF22SA0079616).

AUTHOR CONTRIBUTIONS

Conceptualization, N.D., K.V.L., and J.B.; methodology, N.D., K.V.L., and J.B.; investigation, K.V.L., N.D., and J.B.; writing – review & editing, J.B., N.D., and K.V.L.

DECLARATION OF INTERESTS

The authors declare no competing interests.

DECLARATION OF GENERATIVE AI AND AI-ASSISTED TECHNOLOGIES IN THE WRITING PROCESS

The authors declare that generative AI or AI-assisted technologies were not applied in the writing process.

STAR★METHODS

Detailed methods are provided in the online version of this paper and include the following:

- KEY RESOURCES TABLE
- EXPERIMENTAL MODEL AND STUDY PARTICIPANT DETAILS
  - Collection and processing of GRF
- METHOD DETAILS
  - Glacial rock flour and batch solution
  - Collection of seawater
  - Experimental setup
  - Phytoplankton species and growth media
  - Incubation experiments
- QUANTIFICATION AND STATISTICAL ANALYSIS
  - Model of growth rate and statistical analysis

Received: September 12, 2025
Revised: January 13, 2026
Accepted: April 16, 2026
Published: April 20, 2026

REFERENCES

1. Bennike, O., Jensen, J.B., Sukstorf, F.N., and Rosing, M.T. (2019). Mapping glacial rock flour deposits in Tasersuaq, Southern West Greenland. Geol. Surv. Den. Greenl. Bull. *43*, 1–5. https://doi.org/10.34194/GEUSB-201943-02-06.
2. Sarkar, S.R. (2021). Glacial Rock Flour: Its Characteristic and Enhanced Weathering. PhD Thesis (University of Copenhagen).
3. McGrath, D., Steffen, K., Overeem, I., Mernild, S.H., Hasholt, B., and Van Den Broeke, M. (2010). Sediment plumes as a proxy for local ice-sheet runoff in Kangerlussuaq Fjord, West Greenland. J. Glaciol. *56*, 813–821. https://doi.org/10.3189/002214310794457227.
4. Overeem, I., Hudson, B.D., Syvitski, J.P.M., Mikkelsen, A.B., Hasholt, B., van den Broeke, M.R., Noël, B.P.Y., and Morlighem, M. (2017). Substantial export of suspended sediment to the global oceans from glacial erosion in Greenland. Nat. Geosci. *10*, 859–863. https://doi.org/10.1038/NGEO3046.
5. Andresen, C.S., Karlsson, N.B., Straneo, F., Schmidt, S., Andersen, T.J., Eidam, E.F., Bjørk, A.A., Dartiguemalle, N., Dyke, L.M., Vermassen, F., and Gundel, I.E. (2024). Sediment discharge from Greenland's marine-

terminating glaciers is linked with surface melt. Nat. Commun. *15*, 1332. https://doi.org/10.1038/s41467-024-45694-1.

6. IMBIE Team (2020). Mass balance of the Greenland Ice Sheet from 1992 to 2018. Nature *579*, 233–239. https://doi.org/10.1038/s41586-019-1855-2.
7. Syvitski, J., Ángel, J.R., Saito, Y., Overeem, I., Vörösmarty, C.J., Wang, H., and Olago, D. (2022). Earth's sediment cycle during the Anthropocene. Nat. Rev. Earth Environ. *3*, 179–196. https://doi.org/10.1038/s43017-021-00253-w.
8. Gunnarsen, K.C., Jensen, L.S., Rosing, M.T., and Dietzen, C. (2023). Greenlandic glacial rock flour improves crop yield in organic agricultural production. Nutr. Cycl. Agroecosyst. *126*, 51–66. https://doi.org/10.1007/s10705-023-10274-0.
9. Tingey, S., Wadham, J.L., Telling, J., Flynn, S., Hawkings, J.R., Palinkas, S.S., Mun, Y., Yates, C.A., Lamarche-Gagnon, G., Burford, R., et al. (2025). The potential for glacial flour to impact soil fertility, crop yield and nutrition in mountain regions. iScience *28*, 111476. https://doi.org/10.1016/j.isci.2024.111476.
10. Nielsdóttir, M.C., Moore, C.M., Sanders, R., Hinz, D.J., and Achterberg, E.P. (2009). Iron limitation of the postbloom phytoplankton communities in the Iceland Basin. Glob. Biogeochem. Cycles *23*, GB3001. https://doi.org/10.1029/2008GB003410.
11. Jørgensen, C.J., Søndergaard, J., Larsen, M.M., Kjeldsen, K.K., Rosa, D., Sapper, S.E., Heimbürger-Boavida, L.-E., Kohler, S.G., Wang, F., Gao, Z., et al. (2024). Large mercury release from the Greenland Ice Sheet invalidated. Sci. Adv. *10*, eadi7760. https://doi.org/10.1126/sciadv.adi7760.
12. Krause, J., Zhu, X., Höfer, J., Achterberg, E.P., Engel, A., Meire, L., Stuart-Lee, A.E., and Hopwood, M.J. (2023). Glacier-derived particles as a regional control on marine dissolved Pb concentrations. J. Geophys. Res. Biogeosci. *128*, e2023JG007514. https://doi.org/10.1029/2023JG007514.
13. Hawkings, J., Wadham, J., Tranter, M., Telling, J., Bagshaw, E., Beaton, A., Simmons, S.-L., Chandler, D., Tedstone, A., and Nienow, P. (2016). The Greenland Ice Sheet as a hot spot of phosphorus weathering and export in the Arctic. Glob. Biogeochem. Cycles *30*, 191–210. https://doi.org/10.1002/2015GB005237.
14. Bhatia, M.P., Kujawinski, E.B., Das, S.B., Breier, C.F., Henderson, P.B., and Charette, M.A. (2013). Greenland meltwater as a significant and potentially bioavailable source of iron to the ocean. Nat. Geosci. *6*, 274–278. https://doi.org/10.1038/NGEO1746.
15. Hawkings, J.R., Skidmore, M.L., Wadham, J.L., Priscu, J.C., Morton, P.L., Hatton, J.E., Gardner, C.B., Kohler, T.J., Stibal, M., Bagshaw, E.A., et al. (2020). Enhanced trace element mobilization by Earth's ice sheets. Proc. Natl. Acad. Sci. USA *117*, 31648–31659. https://doi.org/10.1073/pnas.2014378117.
16. Zhu, X., Hopwood, M.J., Laufer-Meiser, K., and Achterberg, E.P. (2024). Incubation experiments characterize turbid glacier plumes as a major source of Mn and Co, and a minor source of Fe and Si, to seawater. Glob. Biogeochem. Cycles *38*, e2024GB008144. https://doi.org/10.1029/2024GB008144.
17. Shoenfelt, E.M., Sun, J., Winckler, G., Kaplan, M.R., Borunda, A.L., Farrell, K.R., Moreno, P.I., Gaiero, D.M., Recasens, C., Sambrotto, R.N., and Bostick, B.C. (2017). High particulate iron(II) content in glacially sourced dusts enhances productivity of a model diatom. Sci. Adv. *3*, e1700314.
18. Bendtsen, J., Daugbjerg, N., and Hansen, J.L.S. (2024). Glacial rock flour increases photosynthesis and biomass of natural phytoplankton communities in subtropical surface waters: a potential means of action for marine CO_2 removal. Front. Mar. Sci. *11*, 1416421. https://doi.org/10.3389/fmars.2024.1416421.
19. Hendry, K.R., Huvenne, V.A.I., Robinson, L.F., Annett, A., Badger, M., Jacobel, A.W., Ng, H.C., Opher, J., Pickering, R.A., Taylor, M.L., et al. (2019). The biogeochemical impact of glacial meltwater from Southwest Greenland. Prog. Oceanogr. *176*, 102126. https://doi.org/10.1016/j.pocean.2019.102126.
20. Jones, R.L., Hawkings, J.R., Meredith, M.P., Lohan, M.C., Moore, O.W., Sherrell, R.M., Fitzsimmons, J.N., Kazemian, M., Araki, T., Kaulich, B., and Annett, A.L. (2025). Antarctic glaciers export carbon-stabilised iron(II)-rich particles to the surface Southern Ocean. Nat. Commun. *16*, 5015. https://doi.org/10.1038/s41467-025-59981-y.
21. Crusius, J., Lao, C.A., Holmes, T.M., and Murray, J.W. (2024). Alaskan glacial dust is an important iron source to surface waters of the Gulf of Alaska. Geophys. Res. Lett. *51*, e2023GL106778. https://doi.org/10.1029/2023GL106778.
22. Gledhill, M., and Buck, K.N. (2012). The organic complexation of iron in the marine environment: a review. Front. Microbiol. *3*, 69. https://doi.org/10.3389/fmicb.2012.00069.
23. Bendtsen, J., Hilligsøe, K.M., Hansen, J.L.S., and Richardson, K. (2015). Analysis of remineralisation, lability, temperature sensitivity and structural composition of organic matter from the upper ocean. Prog. Oceanogr. *130*, 125–145. https://doi.org/10.1016/j.pocean.2014.10.009.
24. Lampe, R.H., Coale, T.H., McQuaid, J.B., and Allen, A.E. (2024). Molecular mechanisms for iron uptake and homeostasis in marine eukaryotic phytoplankton. Annu. Rev. Microbiol. *78*, 213–232. https://doi.org/10.1146/annurev-micro-041222-023252.
25. Gorbunov, M.Y., and Falkowski, P.G. (2022). Using chlorophyll fluorescence to determine the fate of photons absorbed by phytoplankton in the world's oceans. Ann. Rev. Mar. Sci *14*, 213–238. https://doi.org/10.1146/annurev-marine-032621-122346.
26. Twining, B.S., and Baines, S.B. (2013). The Trace Metal Composition of Marine Phytoplankton. Ann. Rev. Mar. Sci *5*, 191–215. https://doi.org/10.1146/annurev-marine-121211-172322.
27. Moore, C.M., Mills, M.M., Arrigo, K.R., Berman-Frank, I., Bopp, L., Boyd, P.W., Galbraith, E.D., Geider, R.J., Guieu, C., Jaccard, S.L., et al. (2013). Processes and patterns of oceanic nutrient limitation. Nat. Geosci. *6*, 701–710. https://doi.org/10.1038/ngeo1765.
28. Ho, T.Y., Quigg, A., Finkel, Z.V., Milligan, A.J., Wyman, K., Falkowski, P.G., and Morel, F.M.M. (2003). The elemental composition of some marine phytoplankton. J. Phycol. *39*, 1145–1159.
29. Harðardóttir, S., Lundholm, N., Moestrup, Ø., and Nielsen, T.G. (2014). Description of Pyramimonas diskoicola sp. nov. and the importance of the flagellate Pyramimonas (Prasinophyceae) in Greenland sea ice during the winter–spring transition. Polar Biol. *37*, 1479–1494. https://doi.org/10.1007/s00300-014-1538-2.
30. Menden-Deuer, S., and Lessard, E.J. (2000). Carbon to volume relationships for dinoflagelllated, diatom, and other protist plankton. Limnol. Oceaongr. *45*, 569–579.
31. Gledhill, M., Van Den Berg, C.M.G., Nolting, R.F., and Timmermans, K.R. (1998). Variability in the speciation of iron in the northern North Sea. Mar. Chem. *59*, 283–300.
32. Dietzen, C., and Rosing, M.T. (2023). Quantification of CO_2 uptake by enhanced weathering of silicate minerals applied to acidic soils. Int. J. Greenhouse Gas Control *125*, 103872. https://doi.org/10.1016/j.ijggc.2023.103872.
33. Hawkings, J.R., Wadham, J.L., Tranter, M., Raiswell, R., Benning, L.G., Statham, P.J., Tedstone, A., Nienow, P., Lee, K., and Telling, J. (2014). Ice sheets as a significant source of highly reactive nanoparticulate iron to the oceans. Nat. Commun. *5*, 3929. https://doi.org/10.1038/ncomms4929.
34. Grider, A., Saros, J., Northington, R., and Yde, J.C. (2025). Glacially-fed lakes of West Greenland have elevated metal and nutrient concentrations and serve as regional repositories of these materials. Sci. Total Environ. *967*, 178744. https://doi.org/10.1016/j.scitotenv.2025.178744.
35. Schroth, A.W., Crusius, J., Hoyer, I., and Campbell, R. (2014). Estuarine removal of glacial iron and implications for iron fluxes to the ocean. Geophys. Res. Lett. *41*, 3951–3958. https://doi.org/10.1002/2014GL060199.
36. Zhang, R., John, S.G., Zhang, J., Ren, J., Wu, Y., Zhu, Z., Liu, S., Zhu, X., Marsay, C.M., and Wenger, F. (2015). Transport and reaction of iron and iron stable isotopes in glacial meltwaters on Svalbard near Kongsfjorden:

From rivers to estuary to ocean. Earth Planet Sci. Lett. *424*, 201–211. https://doi.org/10.1016/j.epsl.2015.05.031.

37. Vives, C.R., Bendtsen, J., Dahms, R.D., Daugbjerg, N., Larsen, K.V., and Rosing, M.T. (2025). Trace metal distributions in the transition zone from the Greenland Ice-Sheet to the surface water in Kangerlussuaq fjord (67 °N). Cryosphere *19*, 3107–3121. https://doi.org/10.5194/tc-19-3107-2025.
38. van Genuchten, C.M., Rosing, M.T., Hopwood, M.J., Liu, T., Krause, J., and Meire, L. (2021). Decoupling of particles and dissolved iron downstream of Greenlandic glacier outflows. Earth Planet Sci. Lett. *576*, 117234. https://doi.org/10.1016/j.epsl.2021.117234.
39. Khoo, C.L.L., Sipler, R.E., Fudge, A.R., Beheshti Foroutani, M., Boyd, S.G., and Ziegler, S.E. (2022). Salt-induced flocculation of dissolved organic matter and iron is controlled by their concentration and ratio in boreal coastal systems. JGR. Biogeosciences *127*, e2022JG006844. https://doi.org/10.1029/2022JG006844.
40. Colombo, M., Rogalla, B., Li, J., Allen, S.E., Orians, K.J., and Maldonado, M.T. (2021). Canadian Arctic Archipelago shelf-ocean interactions: A major iron source to Pacific derived waters transiting to the Atlantic. Glob. Biogeochem. Cycles *35*, e2021GB007058. https://doi.org/10.1029/2021GB007058.
41. Laufer-Meiser, K., Michaud, A.B., Maisch, M., Byrne, J.M., Kappler, A., Patterson, M.O., Røy, H., and Jørgensen, B.B. (2021). Potentially bioavailable iron produced through benthic cycling in glaciated Arctic fjords of Svalbard. Nat. Commun. *12*, 1349. https://doi.org/10.1038/s41467-021-21558-w.
42. Canadell, J.G., Monteiro, P.M.S., Costa, M.H., Cotrim da Cunha, L., Cox, P.M., Eliseev, A.V., Henson, S., Ishii, M., Jaccard, S., Koven, C., et al. (2021). Global Carbon and other Biogeochemical Cycles and Feedbacks. In Climate Change 2021: The Physical Science Basis. Contribution of Working Group I to the Sixth Assessment Report of the Intergovernmental Panel on Climate Change, V. Masson-Delmotte, P. Zhai, A. Pirani, S.L. Connors, C. Péan, S. Berger, N. Caud, Y. Chen, L. Goldfarb, and Gomis., et al., eds. (Cambridge University Press), pp. 673–816. https://doi.org/10.1017/9781009157896.007.
43. Richardson, K., Steffen, W., Lucht, W., Bendtsen, J., Cornell, S.E., Donges, J.F., Drüke, M., Fetzer, I., Bala, G., von Bloh, W., et al. (2023). Earth beyond six of nine planetary boundaries. Sci. Adv. *9*, eadh2458. https://doi.org/10.1126/sciadv.adh2458.
44. Boyd, P.W., and Ellwood, M.J. (2010). The biogeochemical cycle of iron in the ocean. Nat. Geosci. *3*, 675–682. https://doi.org/10.1038/ngeo964.
45. Aumont, O., and Bopp, L. (2006). Globalizing results from ocean in situ iron fertilization studies Global Biogeochem. Cycles *20*, GB2017. https://doi.org/10.1029/2005GB002591.
46. GESAMP (2019). High Level Review of a Wide Range of Proposed Marine Geoengineering Techniques. In IMO/FAO/UNESCO-IOC/UNIDO/WMO/IAEA/UN/UN Environment/UNDP/ISA Joint Group of Experts on the Scientific Aspects of Marine Environmental Protection, *98*, P.W. Boyd and C.M.G. Vivian, eds. (Rep. Stud. GESAMP), p. 144.
47. NASEM, National Academies of Sciences, Engineering, and Medicine (2021). A Research Strategy for Ocean-Based Carbon Dioxide Removal and Sequestration (The National Academies Press). https://doi.org/10.17226/26278.
48. Bendixen, M., Overeem, I., Rosing, M.T., Bjørk, A.A., Kjær, K.H., Kroon, A., Zeitz, G., and Iversen, L.L. (2019). Promises and perils of sand exploitation in Greenland. Nat. Sustain. *2*, 98–104. https://doi.org/10.1038/s41893-018-0218-6.
49. Browning, T.J., and Moore, C.M. (2023). Global analysis of ocean phytoplankton nutrient limitation reveals high prevalence of co-limitation. Nat. Commun. *14*, 5014. https://doi.org/10.1038/s41467-023-40774-0.
50. Wyatt, N.J., Birchill, A., Ussher, S., Milne, A., Bouman, H.A., Shoenfelt Troein, E., Pabortsava, K., Wright, A., Flanagan, O., Bibby, T.S., et al. (2023). Phytoplankton responses to dust addition in the Fe–Mn co-limited eastern Pacific sub-Antarctic differ by source region. Proc. Natl. Acad. Sci. USA *120*, e2220111120. https://doi.org/10.1073/pnas.2220111120.
51. Martin, J.H., Coale, K.H., Johnson, K.S., Fitzwater, S.E., Gordon, R.M., Tanner, S.J., Hunter, C.N., Elrod, V.A., Nowicki, J.L., Coley, T.L., et al. (1994). Testing the iron hypothesis in ecosystems of the equatorial Pacific Ocean. Nature *371*, 123–129.
52. de Baar, H.J.W., Boyd, P.W., Coale, K.H., Landry, M.R., Tsuda, A., Assmy, P., Bakker, D.C.E., Bozec, Y., Barber, R.T., Brzezinski, M.A., et al. (2005). Synthesis of iron fertilization experiments: From the Iron Age in the Age of Enlightenment. J. Geophys. Res. *110*, C09S16. https://doi.org/10.1029/2004JC002601.
53. Boyd, P.W., Jickells, T., Law, C.S., Blain, S., Boyle, E.A., Buesseler, K.O., Coale, K.H., Cullen, J.J., de Baar, H.J.W., Follows, M., et al. (2007). Mesoscale iron enrichment experiments 1993-2005: Synthesis and future directions. Science *315*, 612–617. https://doi.org/10.1126/science.1131669.
54. Harrison, D.P. (2017). Global negative emissions capacity of ocean macronutrient fertilization. Environ. Res. Lett. *12*, 035001. https://doi.org/10.1088/1748-9326/aa5ef5.
55. Siegel, D.A., De Vries, T., Doney, S.C., and Bell, T. (2021). Assessing the sequestration time scales of some ocean-based carbon dioxide reduction strategies. Environ. Res. Lett. *16*, 104003. https://doi.org/10.1088/1748-9326/ac0be0.
56. Tagliabue, A., Twining, B.S., Barrier, N., Maury, O., Berger, M., and Bopp, L. (2023). Ocean iron fertilization may amplify climate change pressures on marine animal biomass for limited climate benefit. Glob. Chang. Biol. *29*, 5250–5260. https://doi.org/10.1111/gcb.16854.
57. Oschlies, A.,, Bach, L.T., Fennel, K., Gattuso, J.-P., and Mengis, N. (2025). Perspectives and challenges of marine carbon dioxide removal. Front. Clim. *6*, 1506181. https://doi.org/10.3389/fclim.2024.1506181.
58. Daugbjerg, N., and Moestrup, Ø. (1992). Ultrastructure of *Pyramimonas cyrtoptera* sp. nov. (Prasinophyceae), a sixteen-flagellate species from Northern Foxe Basin, Arctic Canada, including observations on growth rates. Can. J. Bot. *70*, 1259–1273.
59. Daugbjerg, N., and Moestrup, Ø. (1992). Fine structure of *Pyramimonas cyclotreta* sp. nov. (Prasinophyceae) from Northern Foxe Basin, Arctic Canada, with some observations on growth rates. Eur. J. Protistol. *28*, 288–298.
60. Daugbjerg, N. (2000). *Pyramimonas tychotreta*, sp. nov. (Prasinophyceae), a new marine species from Antarctica: light and electron microscopy of the motile stage and notes on growth rates. J. Phycol. *36*, 160–171.
61. Guillard, R.R.L., and Hargraves, P.E. (1993). Stichochrysis immobilis is a diatom, not a chrysophyte. Phycologia *32*, 234–236. https://doi.org/10.2216/i0031-8884-32-3-234.1.
62. Guillard, R.R.L. (1975). Culture of phytoplankton for feeding marine invertebrates. In Culture of Marine Invertebrate Animals, W.L. Smith and M.H. Chanley, eds. (Plenum Press), pp. 26–60.
63. Gerringa, L.J.A., de Baar, H.J.W., and Timmermans, K.R. (2000). A comparison of iron limitation of phytoplankton in natural oceanic waters and laboratory media conditioned with EDTA. Mar. Chem. *68*, 335–346. https://doi.org/10.1016/S0304-4203(99)00092-4.
64. Oxborough, K. (2021). LabSTAF and RunSTAF Handbook: 2408-014-HB, Issue E. West Molesey, UK (Chelsea Technologies Ltd.), pp. 116.
65. R Core Team (2021). R: A Language and Environment for Statistical Computing (R Foundation for Statistical Computing). https://www.R-project.org/.

STAR★METHODS

KEY RESOURCES TABLE

REAGENT or RESOURCE	SOURCE	IDENTIFIER
Chemicals, peptides, and recombinant proteins		
$NaNO_3$ (concentration in final media: $8.82 \cdot 10^{-4}$ M/L)	Analytical grade	Component in L1-media
$NaH_2PO_4 \cdot H_2O$ (concentration in final media: $3.62 \cdot 10^{-5}$ M/L)	Analytical grade	Component in L1-media
Thiamine·HCL, Vitamin B_1 (concentration in final media: $2.96 \cdot 10^{-7}$ M/L)	Analytical grade	Component in L1-media
Biotin, Vitamin H (concentration in final media: $2.05 \cdot 10^{-9}$ M/L)	Analytical grade	Component in L1-media
Cyanocobalamin, Vitamin B_{12} (concentration in final media: $3.69 \cdot 10^{-10}$ M/L)	Analytical grade	Component in L1-media
$Na_2EDTA \cdot 2H_2O$ (concentration in final media: $1.17 \cdot 10^{-5}$ M/L)	Analytical grade	Component in L1-media
$FeCl_3 \cdot 6H_2O$ (concentration in final media: $1.17 \cdot 10^{-5}$ M/L)	Analytical grade	Component in L1-media
$MnCl_2 \cdot 4H_2O$ (concentration in final media: $9.09 \cdot 10^{-7}$ M/L)	Analytical grade	Component in L1-media
$ZnSO_4 \cdot 7H_2O$ (concentration in final media: $8.00 \cdot 10^{-8}$ M/L)	Analytical grade	Component in L1-media
$CoCl_2 \cdot 6H_2O$ (concentration in final media: $5.00 \cdot 10^{-8}$ M/L)	Analytical grade	Component in L1-media
$CuSO_4 \cdot 5H_2O$ (concentration in final media: $1.00 \cdot 10^{-8}$ M/L)	Analytical grade	Component in L1-media
$Na_2MoO_4 \cdot 2H_2O$ (concentration in final media: $8.22 \cdot 10^{-8}$ M/L)	Analytical grade	Component in L1-media
H_2SeO_3 (concentration in final media: $1.00 \cdot 10^{-8}$ M/L)	Analytical grade	Component in L1-media
$NiSO_4 \cdot 6H_2O$ (concentration in final media: $1.00 \cdot 10^{-8}$ M/L)	Analytical grade	Component in L1-media
Na_3VO_4 (concentration in final media: $1.00 \cdot 10^{-8}$ M/L)	Analytical grade	Component in L1-media
K_2CrO_4 (concentration in final media: $1.00 \cdot 10^{-8}$ M/L)	Analytical grade	Component in L1-media
Lugols Iodine (final concentration 2%)	Analytical grade	Conservation of cells
Experimental models: Organisms/strains		
Pyramimonas diskoicola	Univ. of Copenhagen	Cell culture
Software and algorithms		
R statistical software	R foundation	www.R-project.orrg
Graphpad	GraphPad Prism (v.10.6.0)	www.graphpad.com
Other		
Plankton wheel, 0.5 rpm	Univ. of Copenhagen	Custom made design
Nunc flasks, 25 cm^2	Sarstedt	Incubation bottles
ULM 500	Waltz	Used for PAR measurements
VWR bench pHenomenal	VWR	Used for pH-measurements
Trilogy fluorometer	Turner design	Used for chlorophyll *a* measurements
1 mL Rafter chamber	Sedgewick	Used for cell counting

(*Continued on next page*)

Continued

REAGENT or RESOURCE	SOURCE	IDENTIFIER
Olympus BH2 microscope	Olympus	Used for cell counting
Filtropur V100 Vacuum filter, unit 1000 mL, 0.2 μm	Sarstedt	Used for filtering batch water
Pulverizette 6	Fritz	Planetary monomill for grinding dried GRF
LabSTAF	Chelsea Technologies Ltd	Used for Fv/Fm-measurements
Millipore Synergy UV Water Purification System	Merck Millipore	Ultrapure Milli-Q water used for dilution of batch water

EXPERIMENTAL MODEL AND STUDY PARTICIPANT DETAILS

Collection and processing of GRF

GRF was collected from the same location in 2015 and 2024 (Figure 1). Samples were collected from the surface sediment from a marine deposit in Nuuk fjord (Ilulialik, west Greenland, 64.76°N, 50.66°W) and brought on ship with an excavator in a shallow (~1 m depth) area near a river outlet from a large (~20 km) lake (Tasersuaq) that receives meltwater directly from the Greenland Ice Sheet. Material from 2015 was dried at a dry-room facility, crushed with a jaw-crusher and packed in bags (~25 kg). Samples for experiment 2–4 was collected from the bags. Material from the 2024-material, used in experiment I, was stored in a plastic bag at the site and brought to the laboratory. The wet rock flour was dried at 50°C and grinded with 20 mm Agate grinding bowls (99.9% SiO_2) in a Fritsch pulverizette 6, planetary monomill (2 min, 300 rpm).

METHOD DETAILS

Glacial rock flour and batch solution

Analysis of GRF collected in 2015[2,32] showed a median grain size (d_{50}) ~2.6 μm with a relatively large BET-specific surface area of 19.6 $m^2\ g^{-1}$, and a similar structure was assumed for the 2024-material collected at the same location. The large surface area of the material implies a potential large reactivity with the surrounding environment. GRF from the 2015 batch was collected at the same location as material used in previous studies of marine incubations,[18] terrestrial CO_2-sequestration[32] and growth of crops.[8] The major mineral composition of the GRF used in this experiment consists of biotite, oligoclase/andesine, amphibole, anorthite, quartz, Fe-oxide, K-feldspar, and muscovite.[2,32]

Collection of seawater

Seawater was collected at an open ocean site in the northern North Atlantic in the Icelandic Basin and from a shelf sea at the entrance to the Baltic Sea. Water in the Icelandic Basin was collected at 10 m depth (3 Sep. 2024) from 3 stations between (63.05°*N* 18.21°W) and (63.31°N, 18.19°W). These stations were characterized by low nutrient concentrations ($[PO_4^{3-}]$~0.13 μmol L^{-1}, $[NO_3^-]$~0 μmol L^{-1}). Baltic Sea water was collected in the northern part of The Sound (56.05°N, 12.64°E) at a depth of 32 m. The bottom water was collected at different times during the year. Dissolved inorganic phosphorus and nitrogen concentration vary typically between ~0.5 and 0.7 μM L^{-1} and ~3–7 μM L^{-1}, respectively. It should be noted that the final concentration of N and P in the incubations were much higher due to the addition of L1-media (See key resources table).

Experimental setup

Different combinations of GRF-samples and seawater origin were investigated to identify possible impacts from differences in the processing of GRF-samples and composition of seawater. Experiments were carried out with a green alga incubated on two identical plankton wheels (d = 1 m, rotation of 0.5 rpm) at a constant temperature of 4°C ± 1°C, and exposed to a constant photosynthetically available radiation (PAR = 91 ± 18 μE $m^{-2}\ s^{-1}$ in exp. I-IV, respectively) in a 16:8 h light:dark cycle. These conditions were representative for conditions in a subpolar environment.

Phytoplankton species and growth media

Incubations were made with an arctic green alga *Pyramimonas diskoicola*.[29] Polar species of *Pyramimonas* have optimal temperature for growth in the range of 3°C–8°C.[58–60] An L1 growth media[61] was added to the batch water that contained nitrogen (N), phosphorus (P), and an f/2 vitamin (V) solution.[62] In addition the L1-media contains EDTA. EDTA is included in the growth media to keep the free iron concentration low and comparable to iron in seawater.[63]

L1-media contains 10 compounds of trace metals including Fe and Mn, e.g., iron and manganese was added as $FeCl_3$ and $MnCl_2$ in a concentration of $1.17 \cdot 10^{-5}$ M and $9.09 \cdot 10^{-7}$ M, respectively (key resources table).

A series of treatments were designed for quantifying the biological mobilization rate of Fe, Mn and P (Table 1). A reference treatment with the complete L1-media, i.e., N, P, Vitamins and Trace metals, is referred to as NPVT. This treatment contained sufficient N, P, vitamins and trace metals for several weeks of exponential growth from the initial inoculum of phytoplankton cells. The general sensitivity to trace metals as well as the sensitivity to the Fe-concentration were analyzed. Hence, NPV and NPV + GRF treatments showed the sensitivity between a treatment without any trace metals (i.e., NPV) and a treatment where GRF was added instead of the trace metals. A constant GRF-concentration of 0.326 g L^{-1} was applied in all experiments. This concentration is comparable to high concentrations observed near river outlets in Greenland.[37]

The sensitivity to iron-mobilization from the GRF was analyzed by leaving out iron in the L1-media. Hence, the NPVT-Fe treatment included the full L1-media without iron, and this treatment was compared with NPVT-Fe + GRF, where GRF potentially could compensate for the lack of iron. Similarly, the sensitivity to manganese-mobilization was investigated by omitting Mn in the growth media and comparing NPVT-Mn and NPVT-Mn + GRF treatments. A set of treatments were also analyzed for identifying the potential for P-mobilization from the GRF. The NVT-treatment, i.e., NPVT without P, showed the importance of P for growth during the incubations. This P-limited treatment was then compared with a corresponding set of NPV-treatments where GRF was added (NVT + GRF). Finally, a set of treatments were analyzed with the focus on identifying the possible impact from EDTA in the L1-media on the mobilization rates of iron.

The batch water, i.e., the seawater used in the incubations, was filtered (Filtropur V100 Vacuum filter, 0.2 μm, Sarstedt) and sterilized by autoclaving at 120 °C for 30 min. The N, P and the trace metal solution from the L1-media was included before sterilization. The f/2 vitamin was subsequently added when the L1-media was cooled, and GRF was added at the very start of the experiments. The potential influence of salinity was accounted for by diluting to a common salinity of ∼30 g kg^{-1} with Milli-Q water. Finally, cells of *P. diskoicola* were added in concentrations of ∼10^3 cells mL^{-1} and incubated in 70 mL sterile Nunc-flasks (cell culture flask, 25 cm^2, polystyrene, Sarstedt).

Incubation experiments

All treatments were incubated for 18 to 21 days and measurements were made in the morning every third day. Each sampling was based on triplicate measurements of photosynthetic efficiency determined from variable fluorescence Fv/Fm (LabSTAF, Chelsea Technologies Ltd)[64] after samples were stored in darkness for at least 30 min, and measured in a small sample chamber (20 mL). The Fv/Fm describes the maximum quantum yield of photosystem II, and it expresses the photosynthetic efficiency of the cells where high values indicate cells with a well-functioning photosynthetic apparatus and low Fv/Fm indicates an iron depleted environment.[25] In addition, pH (VWR bench pHenomenal), chlorophyll *a* (Trilogy fluorometer, Turner Design) and salinity (refractometer) were measured. Cell concentrations were attained by manual cell counts from a marked set of triplicates of all treatments and resulted in 3 time series of cell abundances. Cells were counted from 1.175 mL of the incubation sample and stored in Eppendorf tubes with Lugol's iodine (final concentration 2%). Counting of samples used a 1 mL Sedgewick Rafter chambers and an Olympus BH2 microscope. At least 400 cells were counted for each sample.

QUANTIFICATION AND STATISTICAL ANALYSIS

Model of growth rate and statistical analysis

It was assumed that the impact by microbiomes from the small inoculum (∼0.3–1 mL) of the microalgal stock culture or associated with the dried GRF on the cell growth in the sterilized batch water were insignificant for the growth of the cells. Hence, the cell concentration (n, cells mL^{-1}) could be described by a constant growth rate (μ, day^{-1}) as a function of time (t): $n(t) = n(t = 0) \exp(\mu t)$. The growth rate was determined by a linear regression of the logarithm of the cell concentration. Statistical analysis was made with R[65] and GraphPad Prism (ver. 10.6.0) and the significance level was $p = 0.05$.